Rational design of stealthy hyperuniform two-phase media with tunable order

Robert A. DiStasio, Jr.,[1] Ge Zhang,[2] Frank H. Stillinger,[2] and Salvatore Torquato[2,3,*]

[1]*Department of Chemistry and Chemical Biology, Cornell University, Ithaca, New York 14853, USA*

[2]*Department of Chemistry, Princeton University, Princeton, New Jersey 08544, USA*

[3]*Department of Physics, Princeton Institute for the Science and Technology of Materials, and Program in Applied and Computational Mathematics, Princeton University, Princeton, New Jersey 08544, USA*

(Received 4 December 2017; published 27 February 2018)

Disordered stealthy hyperuniform materials are exotic amorphous states of matter that have attracted recent attention because of their novel structural characteristics (hidden order at large length scales) and physical properties, including desirable photonic and transport properties. It is therefore useful to devise algorithms that enable one to design a wide class of such amorphous configurations at will. In this paper, we present several algorithms enabling the systematic identification and generation of discrete (digitized) stealthy hyperuniform patterns with a tunable degree of order, paving the way towards the rational design of disordered materials endowed with novel thermodynamic and physical properties. To quantify the degree of order or disorder of the stealthy systems, we utilize the discrete version of the τ order metric, which accounts for the underlying spatial correlations that exist across all relevant length scales in a given digitized two-phase (or, equivalently, a two-spin state) system of interest. Our results impinge on a myriad of fields, ranging from physics, materials science and engineering, visual perception, and information theory to modern data science.

DOI: 10.1103/PhysRevE.97.023311

I. INTRODUCTION

A hyperuniform state of matter is characterized by an anomalous suppression of density fluctuations at large length scales [1,2]. For example, a hyperuniform many-particle system in d-dimensional space $\mathbb{R}^d$ possesses a local number variance $\sigma^2(R)$ within a spherical observation window of radius R that grows slower than R^d (i.e., window volume) for large R. Equivalently, it is one in which the well-known structure factor $S(\mathbf{k})$ (which is proportional to the scattering intensity [3,4]) tends to zero as the wave number $k \equiv |\mathbf{k}|$ goes to zero, i.e.,

$$\lim_{|\mathbf{k}|\to 0} S(\mathbf{k}) = 0. \tag{1}$$

Hyperuniform systems include all perfect crystals, perfect quasicrystals, and some exotic disordered systems. Typical disordered systems, such as liquids and structural glasses, have variances with the standard volume scaling $\sigma^2(R) \sim R^d$. Figure 1 depicts two disordered non-hyperuniform configurations with different levels of short-range order and two hyperuniform configurations, one disordered and the other ordered.

Disordered hyperuniform patterns are exotic amorphous states of matter poised between perfect crystals and liquids in that they exhibit suppressed large-scale density fluctuations (like perfect crystals) while simultaneously presenting as statistically isotropic with no Bragg peaks (like liquids) [1,2,7,8]. In this sense, hyperuniform systems are characterized by hidden order that is *not* apparent on large length scales [7] and are therefore endowed with several novel thermodynamic and physical properties. To date, these extraordinary states of matter can be found in maximally random jammed particle packings [9–12], jammed athermal granular media [13], jammed thermal colloidal packings [14,15], dynamical states of cold atoms [16], transitions in nonequilibrium systems [17,18], quantum systems [19–21], surface-enhanced Raman spectroscopy [22], terahertz quantum cascade lasers [23], wave dynamics in disordered potentials based on supersymmetry [24], avian photoreceptor patterns [25], as well as certain Coulombic systems [21].

Disordered hyperuniform patterns of the so-called stealthy variety have the additional (and unusual) property of being transparent to radiation across a select range of wavelengths, e.g., $S(\mathbf{k}) = 0$ in a sphere of radius K around the origin $\mathbf{k} = \mathbf{0}$, meaning that they anomalously suppress density fluctuations for these wave vectors. It is noteworthy that there are equilibrium many-particle systems with certain long-range pairwise potentials whose ground states are highly degenerate disordered configurations with these stealthy structure factors [6,7,26]. By mapping such stealthy hyperuniform configurations of particles onto network solids, what was previously thought to be impossible became possible: the rational design of disordered cellular solids that have complete isotropic photonic band gaps comparable in size to photonic crystals [27], thereby providing novel and unexplored ways to manipulate light [28–31]. Moreover, it has recently been shown that disordered stealthy dispersions are endowed with nearly optimal transport properties while being statistically isotropic [32,33]. The fact that stealthy many-particle systems cannot tolerate arbitrarily large holes between the particles [34] is a structural characteristic that is an important factor in bestowing novel properties to disordered stealthy materials [35].

Two-phase heterogeneous media (e.g., composites, porous materials, polymer blends, biological media, suspensions, gels, etc.) represent a very general class of materials, and yet we

*torquato@princeton.edu

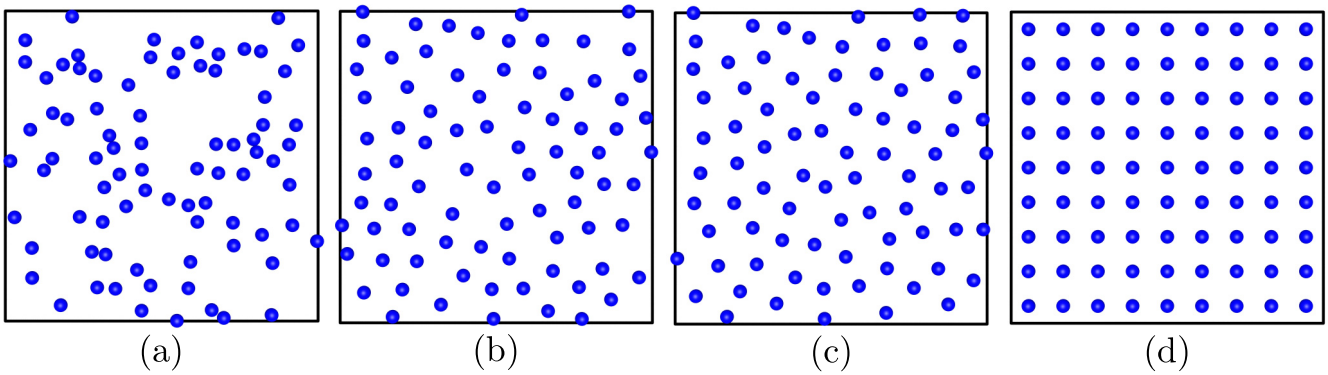

FIG. 1. Graphical depiction of four different many-particle configurations (patterns) that contain varying degrees of structural order, the latter two of which are hyperuniform. (a) Poisson configuration with no discernible short-, intermediate-, or long-range order. (b) Configuration generated via random sequential addition (RSA) with short-range order [5]. (c) Inclusion of very small collective displacements of the particles in (b) to form a hyperuniform configuration [6], a statistically isotropic configuration that contains hidden long-range order yet displays no Bragg peaks. In comparing these two patterns by eye, it can be very difficult to detect the presence of such long-range order in the hyperuniform configuration. (d) Crystalline configuration displaying order across all length scales (and characterized by Bragg peaks).

know little about their existence as stealthy hyperuniform states from a fundamental theoretical perspective. In this paper, we focus our attention on discrete or digitized realizations of two-phase media, since digital images are necessarily pixelized (or voxelized) and modern three-dimensional (3D) printing technologies use digitized data as input, thus providing several immediate and practical applications of the work described herein. Moreover, such digitized systems can be regarded as two-state spin systems. The capability to systematically generate stealthy hyperuniform disordered two-phase heterogeneous media with a tunable degree of order is in its infancy. This work also directly addresses this issue by bringing together aspects of pattern recognition, quantification of order in digitized two-phase media, and the theory of heterogeneous media [36] in the design of a series of algorithms that allow for the systematic identification and generation of digitized stealthy hyperuniform patterns. Accordingly, we design two-phase digitized stealthy hyperuniform patterns with a *tunable* or *prescribed* degree of order. It should be noted that there has been a very recent investigation concerning the design of hyperuniform two-phase materials [33] that complements the approaches that we report in this paper, which is discussed further in Sec. V.

While there is no perfect order metric [37], the existence of stealthy disordered patterns that contain hidden order (i.e., difficult to discern by visual inspection) makes it desirable to utilize an order metric that is able to quantify the degree of order in a given pattern across all relevant length scales. In this work, we introduce and employ a binary-system version of the τ scalar order metric—an order metric that has been fruitfully applied to study translational order across length scales in stealthy point patterns in continuous spaces [7,32]—to rank digitized two-phase patterns. In this regard, the order metric herein can also be viewed as the discrete reciprocal-space analog of the real-space descriptors successfully employed in the inverse reconstruction of two-phase media textures [38].

The remainder of this article is organized as follows. In Sec. II, we provide some necessary mathematical definitions and preliminaries. We introduce in Sec. III the discrete version of the τ order metric and discuss its utility for rank ordering digitized two-phase systems, especially the stealthy variety. In Sec. IV, we present and apply three different numerical procedures to systematically identify and construct digitized stealthy hyperuniform two-phase systems with tunable or prescribed degrees of order: enumeration, stochastic optimization, and superposition procedures. We demonstrate that τ is not only unambiguously consistent with our intuitive notion of order, but can also discriminate subtle textural differences (e.g., hidden order) that exist in discrete stealthy hyperuniform patterns which are not easily discernible by visual inspection. In Sec. V, we make concluding remarks and discuss some implications of our results.

II. MATHEMATICAL DEFINITIONS AND PRELIMINARIES

For concreteness, we focus in this paper on two-dimensional (2D) patterns discretized by (square) binary pixels that are arranged on a square ($\mathbf{Z}^2$) lattice (subject to periodic boundary conditions along the x and y axes). Such patterns can be represented mathematically by $\sigma(m,n)$, a function which takes two integers as input (m and n, the indices specifying the pixel location in the lattice) and yields a binary output (either zero or 1) [39–41]. Accordingly, we can use this formalism to describe *any* two-state system, such as up and down spins (i.e., the Ising model [42,43] for ferromagnetism in statistical mechanics), occupancy and vacancy (i.e., the lattice gas model), or phases A and B in the case of digitized two-phase media.

If L_1 and L_2 are the side lengths (in pixels) for a given pattern, then the total number of pixels is simply given by $N_s = L_1 \times L_2$. This restricts m and n to $1 \leqslant m \leqslant L_1$ and $1 \leqslant n \leqslant L_2$, respectively. Throughout this work, N was chosen to represent the number of up spins or occupied sites [or the phase assigned a value of 1 in $\sigma(m,n)$ for the case of two-phase media] and is therefore given by $N = \sum_{m=1}^{L_1} \sum_{n=1}^{L_2} \sigma(m,n)$. As a result, $f \equiv N/N_s$ will be used to represent the relative fraction of up spins, occupied sites, or a given phase in two-phase media, and is defined in the interval $[0,1]$.

X-ray and neutron-scattering techniques provide powerful ways to probe the structure of matter [3,4]. In this regard,

the static structure factor $S(\mathbf{k})$ encodes such information and has a long-standing tradition as a means for quantifying order (and disorder) in both experiments and simulations. In particular, features such as peaks, rings, and streaks in $S(\mathbf{k})$ are well-established indicators for analyzing the appearance and presence of order in complex materials. Accordingly, $S(\mathbf{k})$ plays a central role in the order metric defined in this work (*vide infra*) and is given by

$$S(\mathbf{k}) = \frac{1}{N}|\widetilde{\rho}(\mathbf{k})|^2. \tag{2}$$

In this expression, we utilize the following discrete form of the collective density variable [6]:

$$\widetilde{\rho}(\mathbf{k}) = \sum_{\text{sites}} \sigma(\mathbf{r}) e^{i\mathbf{k}\cdot\mathbf{r}} = \sum_{m=1}^{L_1}\sum_{n=1}^{L_2} \sigma(m,n) e^{i(k_x m + k_y n)}, \tag{3}$$

with k_x and k_y representing the x and y components of the wave vector $\mathbf{k}$. A digitized pattern will be referred to as "stealthy up to some exclusion radius K" if $S(\mathbf{k}) = 0$ for all $0 < |\mathbf{k}| \leqslant K$. When combined with the definition of $S(\mathbf{k})$ in Eq. (2), this has two important implications that are used throughout this work. First, if a pattern $\sigma_1(m,n)$ is stealthy up to some K, then the inverse of this pattern, $\sigma_2(m,n) \equiv 1 - \sigma_1(m,n)$, is also stealthy up to the same K. This results from the fact that $\widetilde{\rho}_1(\mathbf{k})$ has to vanish for all $0 < |\mathbf{k}| \leqslant K$ when $\sigma_1(m,n)$ is stealthy up to K. In this case, $\widetilde{\rho}_2(\mathbf{k})$ also vanishes for all $0 < |\mathbf{k}| \leqslant K$, from which it follows that $S(\mathbf{k}) = \frac{1}{N}|\widetilde{\rho}_2(\mathbf{k})|^2 = 0$ in this range of $\mathbf{k}$, making $\sigma_2(m,n)$ stealthy up to K as well. Second, if two patterns $\sigma_1(m,n)$ and $\sigma_2(m,n)$ are both stealthy up to some K and $0 \leqslant \sigma_1(m,n) + \sigma_2(m,n) \leqslant 1$ holds for every m and n, then the superposition of these two patterns, $\sigma_3(m,n) = \sigma_1(m,n) + \sigma_2(m,n)$, is also stealthy up to K. This results from the fact that the collective density variables for these two individual patterns are both zero. Since $\widetilde{\rho}_3(\mathbf{k}) = \widetilde{\rho}_1(\mathbf{k}) + \widetilde{\rho}_2(\mathbf{k}) = 0$, $S(\mathbf{k}) = 0$ for $\sigma_3(m,n)$, which makes this pattern also stealthy up to K. We denote such a pattern as "multi-stealthy" since this configuration is comprised of multiple stealthy configurations and note in passing that such a configuration (by definition) is also endowed with the property of being "multi-hyperuniform."

In computing $S(\mathbf{k})$, one only needs to consider a finite number of $\mathbf{k}$-vectors due to the following three reasons. First, the $\mathbf{k}$-vectors need to be consistent with the size of a given pattern, i.e., k_x and k_y must be integer multiples of $2\pi/L_1$ and $2\pi/L_2$, respectively. Second, since $S(\mathbf{k})$ is periodic for the discretized systems considered herein,

$$\begin{aligned} S(k_x + 2\pi, k_y) &= \frac{1}{N}\left|\sum_{m=1}^{L_1}\sum_{n=1}^{L_2}\sigma(m,n)e^{i[(k_x+2\pi)m + k_y n]}\right|^2 \\ &= \frac{1}{N}\left|\sum_{m=1}^{L_1}\sum_{n=1}^{L_2}\sigma(m,n)e^{i(k_x m + k_y n) + i2\pi m}\right|^2 \\ &= \frac{1}{N}\left|\sum_{m=1}^{L_1}\sum_{n=1}^{L_2}\sigma(m,n)e^{i(k_x m + k_y n)}\right|^2 \\ &= S(k_x, k_y), \end{aligned} \tag{4}$$

and similarly, $S(k_x, k_y + 2\pi) = S(k_x, k_y)$, thereby reducing the number of $\mathbf{k}$-vectors via translational symmetry. Furthermore, $S(\mathbf{k})$ for approximately half of these $\mathbf{k}$-vectors are independent variables since [cf. Eqs. (2) and (3)] $S(\mathbf{0}) = N$ and $S(-\mathbf{k}) = S(\mathbf{k})$.

III. QUANTIFYING THE DEGREE OF ORDER IN DISCRETE PATTERNS: THE τ METRIC

Although no perfect order metric necessarily exists [37], many order metrics have been devised to quantify the degree of order or disorder of complex systems at various length scales, including those that account for bond orientations [44,45] and translational order [46,47]. For some of these metrics, the degree of order is referenced to a particular perfect crystalline structure and in other instances a reference state is not assumed. Invariably, all previously employed order metrics incorporate only *spatially local* information in practice.

Here we introduce and apply the discrete-space version of the continuous-space τ order metric that was originally formulated to capture pair correlations of many-particle systems across length scales in Euclidean spaces [7]. The discrete τ metric for a two-phase system with phase volume (occupation) fraction f is defined as

$$\tau[\mathscr{C}] \equiv \sum_{\mathbf{k}\neq\mathbf{0}} [S_{\mathscr{C}}(\mathbf{k}) - S_{\mathscr{P}}(\mathbf{k})]^2 = \sum_{\mathbf{k}\neq\mathbf{0}} [S_{\mathscr{C}}(\mathbf{k}) - (1-f)]^2, \tag{5}$$

in which both summations are over all $\mathbf{k}$-vectors associated with the natural period of the simulation box [excluding the origin ($\mathbf{k} \neq \mathbf{0}$)] and $S_{\mathscr{C}}(\mathbf{k})$ and $S_{\mathscr{P}}(\mathbf{k}) = 1 - f$ are the structure factors, i.e., the Fourier transforms of the corresponding real-space two-point correlation functions [48], for a configuration of interest ($\mathscr{C}$) and an *ensemble* of uncorrelated (Poisson) patterns ($\mathscr{P}$), respectively. We note in passing that τ is also closely related to the two-particle excess entropy [49], since both of these order metrics are defined as integrals over the pair statistics in a given system.

Similar to the continuous case, the order metric defined in Eq. (5) will register large values due to the occurrence of sharp peaks in ordered periodic patterns, which are of finite height in any finite system but become infinite (Dirac δ functions) in the infinite-system-size limit. For finite periodic patterns, one can study how τ grows with the system size. Furthermore, this definition also implies that τ is invariant with respect to trivial symmetry operations, including translations, rotations, and reflections. It is also important to stress here that τ will also register very large values in the vicinity of critical points (e.g., Ising-like critical points [50,51]), due to the fact that $S(\mathbf{k})$ diverges as $\mathbf{k} \to \mathbf{0}$ in the infinite-system-size limit. Hence, while one should exercise caution in interpreting such an order metric in the vicinity of a critical point, τ might also be fruitfully employed to detect whether a disordered system is in fact approaching a critical point. This is a potentially interesting research avenue to explore in the future as all of the examples considered herein are located far away from any critical points.

By defining τ with respect to an ensemble of spatially uncorrelated Poisson point processes, i.e., a collection of random and disordered arrangements of particles that is characterized by $S_{\mathscr{P}}(\mathbf{k}) = 1 - f \;\forall\; \mathbf{k} \neq \mathbf{0}$, τ can also be seen as a

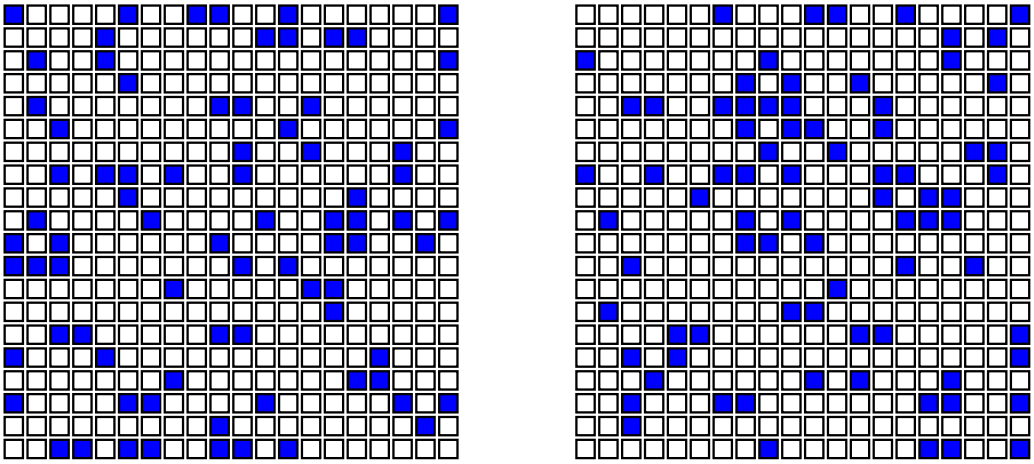

FIG. 2. Graphical depiction of two patterns discretized on a periodic $L \times L$ square lattice (with $L = 20$) comprised of $N = 80$ "particles" (occupied sites) with $f = 0.2$, which are represented by blue squares. While the disordered pattern ($\mathscr{C}$) on the left is hyperuniform and stealthy for an exclusion radius of $K = 1$ (in units of $2\pi/L$), the disordered pattern ($\mathscr{P}$) on the right is simply an uncorrelated (Poisson) pattern that, of course, is neither stealthy nor hyperuniform. The stealthy hyperuniform pattern was generated using the stochastic optimization method described in Sec. IV B. This figure demonstrates that while stealthy hyperuniform patterns look very similar to uncorrelated patterns at short range, they contain hidden long-range order (i.e., suppression of large-scale number density fluctuations) that is not easily detectable by eye. Since $\tau[\mathscr{C}]/\tau[\mathscr{P}] = 3/2$, the τ order metric quantitatively illustrates the fact that this disordered stealthy hyperuniform configuration—purely through the presence of hidden long-range order—is indeed significantly more ordered than the uncorrelated pattern.

reciprocal-space analog of the real-space descriptors successfully employed in the inverse reconstruction [38] of two-phase media textures. Such textures are of importance across a wide variety of fields, ranging from the microscopic length scales encountered in materials science (e.g., the microstructure of sandstones, metal-ceramic composites, and concrete) and systems biology (e.g., the structure of plant and animal tissues, cell aggregates, and medical imaging) to the macroscopic length scales found in ecology (e.g., distributions of trees in forests) and cosmology (e.g., galaxy distributions and stellar constellations).

As seen in Eq. (5), τ accumulates the deviation of $S_{\mathscr{C}}(\mathbf{k})$ from $1 - f$ for all $\mathbf{k} \neq \mathbf{0}$ (in a single period as defined by the $\mathbf{k}$-point mesh required to accurately sample a square lattice with a spatial extent of length $L_1 \times L_2$), thereby providing an unbiased estimate of the order contained within a given discrete pattern by equally accounting for contributions across short-, intermediate-, and long-range distances. As such, τ is therefore of particular importance in the discrimination of stealthy hyperuniform configurations—patterns which are characterized by the presence of hidden long-range order arising from the suppression of number density fluctuations on large length scales. As seen in Fig. 2, such patterns are often difficult, if not impossible, to detect by eye, as the contrast sensitivity of human vision peaks at fairly short distances [52], thereby placing a larger relative weight on observed textural similarities (or lack thereof) in this portion of the distance spectrum. This limitation is overcome by the use of the τ order metric: by quantitatively detecting the presence of order across all length scales, τ can easily discern a disordered stealthy hyperuniform configuration from a random Poisson point pattern.

The strength and utility of τ as a quantitative and unbiased estimator of the degree of order in a given discretized pattern lies in the fact that τ not only agrees with our intuitive definition of order in unambiguous textural comparisons (i.e., by clearly differentiating significantly ordered crystalline structures from disordered Poisson configurations) but can also discriminate subtle textural differences that are not so easily discernible by visual inspection (i.e., by clearly differentiating disordered patterns that contain some degree of hidden order, such as the aforementioned class of stealthy hyperuniform configurations, from truly random spatially uncorrelated Poisson patterns). Moreover, the fact that this discrete version of τ has also been used to uncover hidden multiscale order in the prime numbers [53] is a strong indication of its utility as an order metric.

IV. DESIGN OF STEALTHY HYPERUNIFORM DIGITIZED TWO-PHASE MEDIA WITH TUNABLE ORDER

A. Enumeration procedure

Here, we explicitly investigate all the possible patterns that can exist on the 2D square lattice with side lengths $L_1 = L_2 = L \in \{3,4,5,6\}$, subject to standard periodic boundary conditions along both axes. Unlike the case of continuous point-particle systems, for which the configurations that can exist comprise an uncountable infinite set, the systems considered herein have a discrete number of degrees of freedom due to the fact that each lattice site is binary and can either be occupied by a particle or vacant (unoccupied). As such, there exists a finite number of possible patterns that can be discretized on a square lattice of side length L, namely $2^{L\times L}$, and each configuration must be enumerated to obtain an accurate count of the number of stealthy hyperuniform patterns that exist on these underlying lattices. The largest system considered was the 6×6 square lattice, which required explicit enumeration of $2^{36} = 6.9 \times 10^{10}$ configurations. For each configuration, the corresponding structure factor, $S(\mathbf{k})$, was computed for the smallest $\mathbf{k}$-vectors contained in the reciprocal-space (k-point) mesh, namely, $\mathbf{k}_1 = [1,0]$ and $\mathbf{k}_2 = [0,1]$, as $S(\mathbf{k}_1) = S(\mathbf{k}_2) = 0$ is the minimal requirement for classification as a stealthy

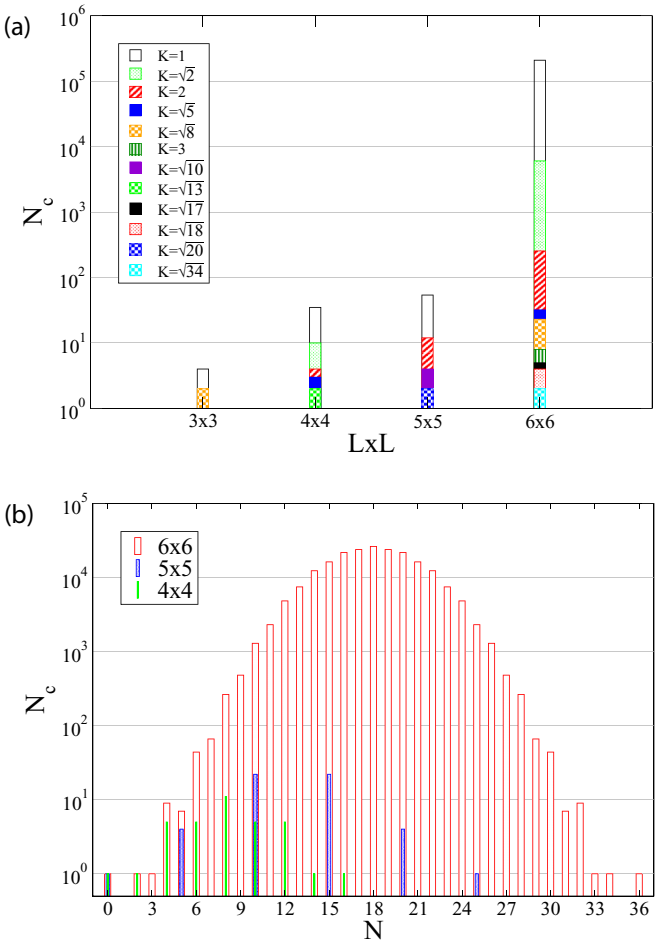

FIG. 3. The number of distinct stealthy hyperuniform patterns identified by an exhaustive enumeration of the discrete patterns existing on a periodic $L \times L$ square lattice (with $L \in \{3,4,5,6\}$), sorted by (a) L and K (in units of $2\pi/L$) and (b) L and N.

hyperuniform pattern (with a corresponding exclusion radius of $K = 1$). Each time a configuration met this criterion, it was added to a running list of stealthy hyperuniform configurations (that was maintained throughout the execution of the enumeration algorithm) and explicitly compared against all other structures on the list to remove trivial configurational degeneracies due to symmetrical equivalence (via the set of translations, rotations, and reflections defined by the periodicity of the underlying lattice). The final list of nonredundant and symmetry-unique configurations constituted the set of existing stealthy hyperuniform configurations for a given lattice [40].

The results of this enumeration study are summarized in Fig. 3. As L increases, Fig. 3(a) shows that the number of unique configurations that are stealthy up to a certain K also increases, as expected. However, the growth increments are not uniform. For instance, the number of configurations that are stealthy up to $K = 1$ increases dramatically when L increases from 5 to 6, but not as much when L is increased from 4 to 5. This nonuniformity is caused by the underlying relationship between the prime factorization of L and the set of N values that can admit stealthy hyperuniform configurations. As Fig. 3(b) shows, only the N values that are integer multiples of 5 admit stealthy configurations for $L = 5 = 1 \times 5$. For $L = 4 = 2 \times 2$, only the N values that are multiples of 2 admit stealthy configurations. The $L = 6 = 2 \times 3$ case, however, is much richer. The set of allowed N values not only includes multiples of 2 and 3, but also includes sums of multiples of 2 and 3. As a result, N can have any value between zero and 6×6, except 1 and 35. Here, the exception for $N = 1$ is due to the fact that 1 is not a sum of a multiple of 2 and 3. The exception for $N = 35$ follows from the fact that this case is the inverse of $N = 1$. Compared to the $L = 5$ case, the $L = 6$ case allows many more N choices and therefore produces a drastically increased number of stealthy patterns. We note in passing that Fig. 3(b) also shows that the distribution of N in the stealthy hyperuniform configurations is roughly a Gaussian (a parabola in our semilogarithmic plot) centered at $N = L^2/2$.

Figure 4 shows a series of discretized patterns obtained via an exhaustive enumeration of the configurational space corresponding to a periodic 6×6 square lattice: six representative stealthy hyperuniform patterns [in which $S(\mathbf{k}) = 0$ for some positive exclusion radius, $K \geqslant 1$, in units of $2\pi/L$ throughout the paper] are arranged from most to least ordered according to their respective τ values. From this figure, it is clear that the crystalline striped-phase and simple checkerboard configurations represent the most ordered stealthy hyperuniform patterns that can be discretized on a 6×6 square lattice, a fact that is appropriately reflected in their computed order metric values of $\tau = 1.000$ and relatively large exclusion radii of $K = 3$ and $K = 3\sqrt{2}$, respectively. With an order metric value of $\tau = 0.390$, the staircase configuration is visibly less ordered than the configurations on the left, and is also accompanied by a smaller exclusion radius of $K = \sqrt{5}$.

More importantly, the success of τ extends well beyond visually detectable ranges of order. For the three remaining stealthy hyperuniform configurations in Fig. 4, all of which have an exclusion radius of $K = 1$, it becomes increasingly more difficult to discern the level of order (or lack thereof) in these patterns by eye. In this regard, a careful visual examination of the configuration characterized by $\tau = 0.110$ reveals that this pattern can be constructed via the introduction of several defects (i.e., replacements of select occupied sites by vacancies) into the simple checkerboard pattern, a fact which is quantitatively captured by τ. However, the fact that the two remaining stealthy hyperuniform configurations on the right of Fig. 4 *appear* as patterns that contain no apparent or discernible order is an inaccurate assessment of these configurations. When compared to the aforementioned crystalline configurations, these two patterns are visibly more disordered, a fact which is again quantitatively reflected by the relatively lower value of $\tau = 0.012$ computed for each of these configurations. In the same breath, these two patterns are indeed stealthy hyperuniform configurations [with $S(\mathbf{k}) = 0$ for $K = 1$] and, as such, these patterns contain some degree of hidden long-range order that is not present in a spatially uncorrelated Poisson pattern, an example of which is given on the far right of Fig. 4, wherein $S(\mathbf{k}) \neq 0$ for $K = 1$.

B. Stochastic optimization algorithm

In this work, we also utilized the simulated annealing (SA) global optimization scheme [54] in conjunction with classi-

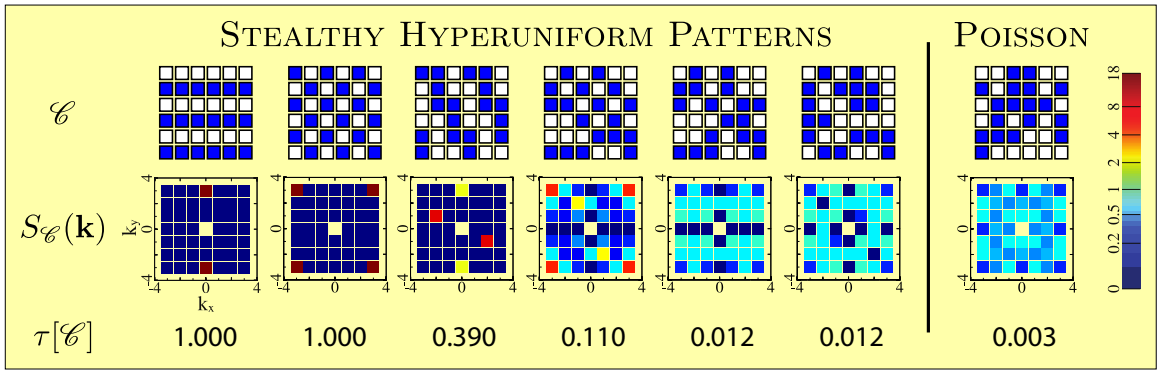

FIG. 4. Top: Graphical depiction of a representative series of six stealthy hyperuniform configurations and a single uncorrelated (Poisson) configuration discretized on a periodic $L \times L$ square lattice (with $L = 6$). Each of these configurations, $\mathscr{C}$, is comprised of $N = 18$ particles (which corresponds to an occupancy of $f = 18/36 = 0.5$) that are represented by blue squares. Middle: Corresponding structure factors, $S_{\mathscr{C}}(\mathbf{k})$, for each configuration. For the six stealthy hyperuniform configurations, $S_{\mathscr{C}}(\mathbf{k}) = 0$ for some positive exclusion radius, $K \geqslant 1$ (in units of $2\pi/L$), a property which is not shared by the spatially uncorrelated Poisson pattern on the far right. Bottom: Corresponding order metric values, $\tau[\mathscr{C}]$, for each configuration as defined by Eq. (5). Note that these patterns have been arranged from most ordered to least ordered, based on the computed values of $\tau[\mathscr{C}]$. These values have been normalized based on the τ measures for the most ordered configuration on the 6×6 square lattice, *i.e.*, the striped or checkerboard configuration.

cal (Metropolis-Hastings) Monte Carlo (MC) simulations to generate stealthy hyperuniform configurations discretized on square lattices that were too large for an exhaustive enumeration study. For a given trial configuration, $\mathscr{C}$, the fictitious energy (or objective function) employed in these SA-MC simulations was chosen to be

$$\theta[\mathscr{C}] = \sum_{\mathbf{k},0<|\mathbf{k}|\leqslant K} [S_{\mathscr{C}}(\mathbf{k}) - S_{\mathscr{T}}(\mathbf{k})]^2 = \sum_{\mathbf{k},0<|\mathbf{k}|\leqslant K} [S_{\mathscr{C}}(\mathbf{k})]^2, \tag{6}$$

in which $S_{\mathscr{C}}(\mathbf{k})$ and $S_{\mathscr{T}}(\mathbf{k})$ are the corresponding structure factors for $\mathscr{C}$ and a *target* ($\mathscr{T}$) configuration, respectively, and the summations are carried out over all $\mathbf{k}$ for which $0 < |\mathbf{k}| \leqslant K$, based on a predefined exclusion radius K. Since our goal is to use SA-MC to stochastically generate stealthy hyperuniform configurations, we take $\mathscr{T}$ to represent a fictitious target stealthy hyperuniform configuration that is characterized by $S_{\mathscr{T}}(\mathbf{k}) = 0 \; \forall \; \{\mathbf{k} \mid 0 < |\mathbf{k}| \leqslant K\}$. Quite interestingly, this objective function is a direct analog of τ, demonstrating the utility of this order metric in the first systematic design of stealthy hyperuniform two-phase digitized patterns with prescribed degrees of order.

The simple quadratic functional form for θ in Eq. (6) is therefore minimized once a configuration $\mathscr{C}$ is located with $S_{\mathscr{C}}(\mathbf{k}) = 0$ for all $\mathbf{k}$-vectors contained within the aforementioned exclusion radius, thereby yielding a stealthy hyperuniform configuration with a prescribed degree of order. Due to the presence of "multiple minima" on these high-dimensional PESs, which hinders the success rate of global optimization techniques such as SA-MC, we applied a logarithmic transformation on the objective function, i.e., $\overline{\theta} = \log_{10}(\theta)$, to clearly differentiate the energy scales associated with global and local minima. As Fig. 5 shows, this logarithmic transformation drastically improves the depth of the ground-state energy basins, making them much more favorable at lower temperatures. A true ground state (in this case a stealthy hyperuniform pattern) should have $\theta = 0$ or $\overline{\theta} = -\infty$. Due to machine precision (double precision arithmetic was employed throughout this work), the evaluated $\overline{\theta}$ is often around -60. Based on this observation, we considered a SA-MC run to be successful in generating a stealthy hyperuniform configuration once $\overline{\theta}[\mathscr{C}] < -50$ (which corresponds to $\theta[\mathscr{C}] < 10^{-50} \approx 0$).

During the SA-MC optimizations, the temperature T was slowly decreased using an exponential cooling schedule, i.e., $T = \exp(-3 \times 10^{-7} N_t/N)$, in which N_t is the number of trial MC moves attempted (at a given T) and N is the number of particles (or occupied sites), until $T = T_{\min} < 0.1$. To allow for finer refinements of the trial configuration and further minimization of the fictitious energy, an additional $2000N$ trial MC moves were attempted at $T = 0$. Initially, the trial MC moves consist of swapping a randomly chosen occupied site with a randomly chosen unoccupied site. However, the acceptance ratio for this specific type of trial MC move becomes too low as T decreases (i.e., the system is not exploring configurational space and is essentially stuck). To remedy this issue, we switched to "local" trial MC moves

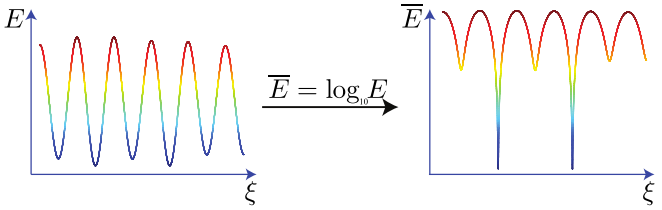

FIG. 5. Graphical depiction of a one-dimensional slice through a high-dimensional potential energy surface (PES) before (left) and after (right) the application of a logarithmic transformation on the energy, E, i.e., $\overline{E} = \log_{10}(E)$, as a function of the configurational coordinate, ξ. The existence of multiple minima in such high-dimensional PES (depicted here by the presence of two degenerate *global* minima in the vicinity of three low-lying and nearly degenerate *local* minima) plagues global optimization techniques such as simulated annealing (SA) and can be significantly alleviated via the application of this logarithmic transformation on the objective function.

TABLE I. Success rates for generating stealthy hyperuniform configurations via simulated annealing Monte Carlo (SA-MC) simulations as a function of N and K on a 10×10 square lattice. For each N and K, 1000 independent SA-MC runs were attempted to determine the final success rate.

f	Success rate for $K =$					
	1	$\sqrt{2}$	2	$\sqrt{5}$	$\sqrt{8}$	3
0.1	1.000	1.000	0.980	1.000	0.999	0.989
0.2	0.995	0.987	0.158	0.001	0.000	0.000
0.3	0.993	0.771	0.047	0.000	0.000	0.000
0.4	0.993	0.726	0.039	0.000	0.000	0.000
0.5	0.989	0.600	0.007	0.000	0.000	0.000

once the acceptance ratio dips below a preset threshold of $A_{\min} = 0.1$ (i.e., less than 1000 accepted moves per 10 000 trial moves). These local trial MC moves involved swapping a randomly chosen occupied site with a randomly chosen unoccupied site that is located within a specified cutoff distance (usually set to approximately three to four units in the lattice spacing). Furthermore, we also gradually decrease this cutoff distance thereafter (until it reaches one unit in the lattice spacing) to maintain an acceptance ratio above $A_{\min}$. These algorithmic details and associated parameters were primarily determined through a trial-and-error approach that maximized the success rate and computational efficiency of this stochastic optimization procedure. Here we stress again that the logarithmic transformation described above plays a critical role in locating stealthy hyperuniform patters via SA-MC simulations, where one is faced with a PES that is plagued with multiple nearly degenerate minima (see Fig. 5).

The success rate for our SA-MC program on a 10×10 lattice ($L = 10$) is summarized in Table I for $f = N/L^2 \leqslant 0.5$. Since our numerical method treats occupied sites and unoccupied sites symmetrically, the success rate for $f = x > 0.5$ should be equal to the success rate for $f = 1 - x$. As f approaches 0.5, the observed decrease in the success rate is most likely due to the fact that the search space, i.e., the number of configurations with a particular N, given by $(L^2)!/[N!(L^2 - N)!]$, is largest for $f = 0.5$. In this regard, it would be interesting to find robust alternative methods for overcoming this numerical difficulty and one such approach is presented below. Four configurations (with $f = 0.2$) identified using this SA-MC method are shown in Fig. 6. The annealed configurations are disordered for the smaller three K values, but crystalline for $K = \sqrt{5}$. We note here that this disorder-to-order transition with increasing K was also observed in continuous stealthy hyperuniform systems [6].

C. Stealthy designs via superposition

To find stealthy hyperuniform patterns for a particular system size and N, one can simply enumerate all possible configurations if the system size is small and use SA-MC for larger systems if N is small. That leaves us with the following question: what method should one use if the system size and N are both large? Here we present one such method, which involves a superposition of stealthy hyperuniform patterns with smaller N values. As discussed above, if two patterns $\sigma_1(m,n)$ and $\sigma_2(m,n)$ are both stealthy up to some K and $\sigma_3(m,n) = \sigma_1(m,n) + \sigma_2(m,n)$ is always between zero and 1 (i.e., there is no overlap in a given phase between the two configurations), then $\sigma_3(m,n)$ is also stealthy up to K. As such, we simply identify "building block" patterns with relatively small N values and then translate them to eliminate overlaps before superposition.

Figure 7 contains several examples of stealthy hyperuniform patterns (up to $K = 1$) that have been generated using

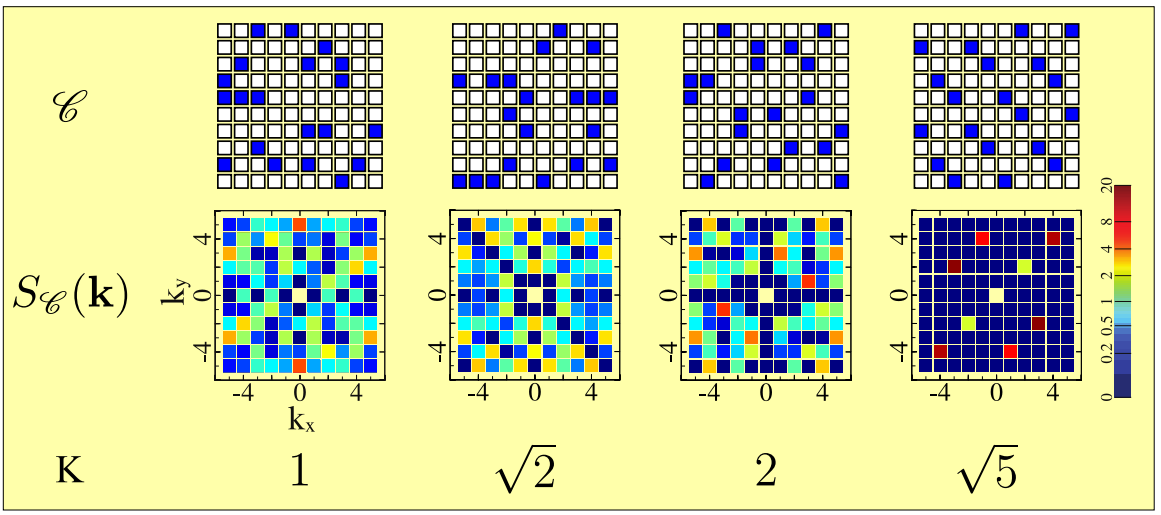

FIG. 6. Top: Graphical depiction of a representative series of stealthy hyperuniform patterns generated using our SA-MC approach. Each of these stealthy patterns is discretized on a periodic 10×10 square lattice and comprised of $N = 20$ particles ($f = 0.2$). Middle: Corresponding structure factors, $S(\mathbf{k})$, for each stealthy pattern in which $S(\mathbf{k}) = 0$ for some positive exclusion radius, $K \geqslant 1$. Bottom: Corresponding exclusion radii, K, for each stealthy pattern. Note that these stealthy patterns have been arranged in increasing order based on the values of K. The corresponding τ order metric values (normalized here by N^2) for each of these stealthy patterns were computed as 0.18, 0.19, 0.33, and 2.59, respectively, indicating that τ and K are again positively correlated in these instances.

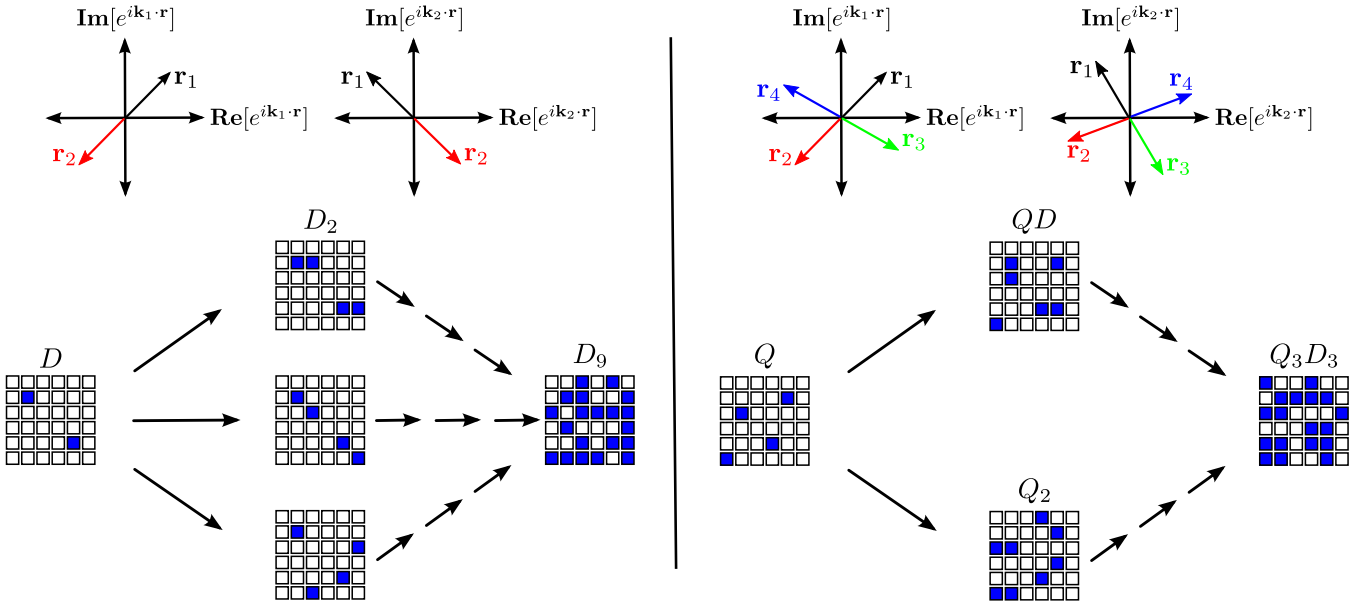

FIG. 7. Top left: Vectorial representation of a stealthy pattern comprised of $N = 2$ particles. The corresponding structure factor, $S(\mathbf{k}) = \frac{1}{N}|\sum_{j=1}^{N}\exp[i\mathbf{k}\cdot\mathbf{r}_j]|^2$, will vanish at a given pair of $\mathbf{k}$-vectors, $\mathbf{k}_1$ and $\mathbf{k}_2$, when $\mathbf{r}_1$ and $\mathbf{r}_2$ satisfy the following equations: (1) $\exp[i\mathbf{k}_1\cdot\mathbf{r}_1] + \exp[i\mathbf{k}_1\cdot\mathbf{r}_2] = 0$ and (2) $\exp[i\mathbf{k}_2\cdot\mathbf{r}_1] + \exp[i\mathbf{k}_2\cdot\mathbf{r}_2] = 0$. Any set of $N = 2$ particles whose coordinates satisfy these constraints constitutes a doublet (D). Bottom left: Graphical depiction of a series of stealthy patterns discretized on a periodic 6×6 square lattice that were constructed via superposition of multiple doublets (i.e., $D_2 = D \oplus D$ and $D_9 = D \oplus D \oplus \cdots \oplus D$). Since *each* doublet constitutes a stealthy pattern, the superposition of multiple doublets (without overlap) constitutes a stealthy (or multi-stealthy) hyperuniform pattern as well. Top right: Vectorial representation of a stealthy pattern comprised of $N = 4$ particles. The corresponding structure factor will vanish at a given pair of $\mathbf{k}$-vectors, $\mathbf{k}_1$ and $\mathbf{k}_2$, when $\mathbf{r}_1$, $\mathbf{r}_2$, $\mathbf{r}_3$, and $\mathbf{r}_4$ satisfy the following equations: (1) $\exp[i\mathbf{k}_1\cdot\mathbf{r}_1] + \exp[i\mathbf{k}_1\cdot\mathbf{r}_2] = 0$, (2) $\exp[i\mathbf{k}_1\cdot\mathbf{r}_3] + \exp[i\mathbf{k}_1\cdot\mathbf{r}_4] = 0$, (3) $\exp[i\mathbf{k}_2\cdot\mathbf{r}_1] + \exp[i\mathbf{k}_2\cdot\mathbf{r}_3] = 0$, and (4) $\exp[i\mathbf{k}_2\cdot\mathbf{r}_2] + \exp[i\mathbf{k}_2\cdot\mathbf{r}_4] = 0$. Any set of $N = 4$ particles whose coordinates satisfy these constraints constitutes a quartet (Q). Note here that a quartet is not simply a pair of doublets, i.e., $Q \neq D_2 = D \oplus D$. Bottom right: Graphical depiction of a series of stealthy patterns discretized on a periodic 6×6 square lattice that were constructed via superposition of multiple doublets and quartets (i.e., $QD = Q \oplus D$, $Q_2 = Q \oplus Q$, and $Q_3D_3 = Q \oplus Q \oplus Q \oplus D \oplus D \oplus D$). Since *each* doublet and *each* quartet constitute a stealthy pattern, the superposition of multiple doublets and quartets (without overlap) constitutes a stealthy (or multi-stealthy) hyperuniform pattern as well. Hence, this superposition technique can be utilized to directly generate stealthy patterns with both large L and N.

this superposition technique. We chose $L = 6$ for visual clarity, but the method is equally (and particularly) suitable for larger systems. For this system size and K, our enumeration study found one stealthy configuration with $N = 2$ and nine stealthy configurations with $N = 4$. The configuration with $N = 2$ is denoted as a doublet (D) and represents the smallest building block in this superposition scheme. Of the nine $N = 4$ configurations, five of them can be decomposed as superpositions of pairs of doublets, denoted by $D_2 = D \oplus D$ as a doublet of doublets. The remaining four configurations with $N = 4$ are therefore quartets (Q). As Fig. 7 illustrates, we can superpose these doublet and quartet building blocks to create complex stealthy hyperuniform patterns. For example, by superposing nine doublets one can create the configuration labeled D_9 in Fig. 7 and by superposing three quartets and three doublets, one can create the configuration labeled Q_3D_3. For a configuration generated by this superposition technique to be stealthy up to a given K value, $S(\mathbf{k})$ at two different $\mathbf{k}$-vectors is constrained to be zero. Figure 7 also demonstrates how D and Q building blocks satisfy these constraints.

V. DISCUSSION

In summary, we have devised several algorithms and methods that enable the systematic identification and generation of digitized stealthy hyperuniform patterns with machine-level precision with a tunable or prescribed degree of order. Thus, our work provides a platform to explore their potentially novel thermodynamic and physical properties that are only beginning to emerge in condensed matter physics, materials science, and engineering [26,27,29–33]. Our work brings together the quantification of order in digitized two-phase media and the theory of heterogeneous media [36]. It is noteworthy that our stealthy designs can easily be fabricated using 3D printing technologies [55].

It is instructive to remark on the related work by Chen and Torquato [33] that was mentioned in the Introduction. These authors demonstrated that one can construct hyperuniform two-phase systems with a prescribed (targeted) "spectral density" (directly related to the structure factor of a digitized system) with relatively high precision by performing simulated annealing with an energy defined as the sum of the squared error from the target. This procedure can produce nearly stealthy two-phase media if the target is set to zero in a certain range near the origin. In this paper, we generate stealthy two-phase media with a more precise requirement for the stochastic optimization algorithm: $S(k)$ is exactly zero when calculated analytically, or $S(k)$ is on the order of machine precision when calculated numerically. As we have seen in this paper, this increase in required precision greatly reduces the system

sizes this method can handle. This motivated us to explore other methods (enumeration and superposition procedures) to generate such *exactly* stealthy hyperuniform systems.

Our work highlights the strength and utility of the τ order metric to detect order in a given digitized two-phase configuration at short-, intermediate-, and long-range distances, especially its ability to detect hidden order in stealthy hyperuniform systems. We have already noted that it has been recently employed to uncover hidden multiscale order in the spatial distribution of the prime numbers [53]. These results suggest that this order metric could be fruitfully employed across a myriad of fields, including visual perception [56], digital image processing and complex pattern recognition (e.g., facial and voice recognition, linguistics, and lexical similarity) [57], information theory (e.g., Shannon entropy, cryptography, and encoding) [58–61], as well as data-intensive statistical efforts such as supervised and unsupervised machine learning. In this regard, τ (or appropriate modifications thereof) could be employed in pattern recognition algorithms to identify and quantitatively discern textural similarities and differences that exist across all length scales relevant to the problem at hand. While the Fourier transform is the basic mathematical operation underlying the definition of τ, alternative order metric definitions which utilize different integral transformations should also be considered. One such direction could involve "wavelets" [62]. The central comparison issue here would be whether or not such an alternative strategy manages to produce equal sensitivity to short-, intermediate-, and long-range patterns or textures.

We expect that the generalization of the methods and algorithms presented herein to the rational design of 3D stealthy hyperuniform patterns with tunable order will be extremely useful and warrants further research. In this regard, the extension of the underlying mathematical formalism in Sec. II is very straightforward and simply requires an additional dimension in $\sigma(m,n)$ [and therefore an additional sum in Eq. (3) for the collective density variable]. However, the three algorithms introduced in this work will have significantly different levels of computational complexity as the spatial dimension increases. For one, the explicit enumeration technique in Sec. IV A will have the worst computational scaling (i.e., the number of configurations that will need to be considered goes from $2^{L_1\times L_2}$ in two dimensions to $2^{L_1\times L_2\times L_3}$ in three dimensions), thereby limiting its domain of applicability to even smaller systems in three dimensions. On the other hand, both the stochastic optimization algorithm (Sec. IV B) and the superposition procedure (Sec. IV C) will work better in 3D as their associated computational complexities are constant with an increase in the spatial dimension. Accordingly, we expect that these algorithms will be quite useful in extending our ability to design textures with tunable multi-scale order in three dimensions.

ACKNOWLEDGMENTS

R.D. acknowledges partial support from Cornell University through start-up funding and the Cornell Center for Materials Research (CCMR) with funding from the National Science Foundation MRSEC program (Grant No. DMR-1719875). G.Z. and S.T. acknowledge the partial support of the National Science Foundation under Grant No. CBET-1701843. This research used resources of the Argonne Leadership Computing Facility at Argonne National Laboratory, which is supported by the Office of Science of the U.S. Department of Energy under Contract No. DE-AC02-06CH11357. This research also used resources of the National Energy Research Scientific Computing Center, which is supported by the Office of Science of the U.S. Department of Energy under Contract No. DE-AC02-05CH11231. Additional computational resources were provided by the Terascale Infrastructure for Groundbreaking Research in Science and Engineering (TIGRESS) High Performance Computing Center and Visualization Laboratory at Princeton University.

[1] S. Torquato and F. H. Stillinger, Local density fluctuations, hyperuniform systems, and order metrics, Phys. Rev. E **68**, 041113 (2003).

[2] C. E. Zachary and S. Torquato, Hyperuniformity in point patterns and two-phase heterogeneous media, J. Stat. Mech. Theor. Exp. (2009) P12015.

[3] J. P. Hansen and J. R. McDonald, *Theory of Simple Liquids*, 3rd ed. (Academic, New York, 2005).

[4] N. W. Ashcroft and N. D. Mermin, *Solid State Physics*, 1st ed. (Holt, Rinehart and Winston, New York, 1976).

[5] G. Zhang and S. Torquato, Precise algorithm to generate random sequential addition of hard hyperspheres at saturation, Phys. Rev. E **88**, 053312 (2013).

[6] O. U. Uche, F. H. Stillinger, and S. Torquato, Constraints on collective density variables: Two dimensions, Phys. Rev. E **70**, 046122 (2004).

[7] S. Torquato, G. Zhang, and F. H. Stillinger, Ensemble Theory for Stealthy Hyperuniform Disordered Ground States, Phys. Rev. X **5**, 021020 (2015).

[8] S. Torquato, Disordered hyperuniform heterogeneous materials, J. Phys.: Condens. Matter **28**, 414012 (2016).

[9] A. Donev, F. H. Stillinger, and S. Torquato, Unexpected Density Fluctuations in Disordered Jammed Hard-Sphere Packings, Phys. Rev. Lett. **95**, 090604 (2005).

[10] C. E. Zachary, Y. Jiao, and S. Torquato, Hyperuniform Long-Range Correlations Are a Signature of Disordered Jammed Hard-Particle Packings, Phys. Rev. Lett. **106**, 178001 (2011).

[11] Y. Jiao and S. Torquato, Maximally random jammed packings of Platonic solids: Hyperuniform long-range correlations and isostaticity, Phys. Rev. E **84**, 041309 (2011).

[12] D. Chen, Y. Jiao, and S. Torquato, Equilibrium phase behavior and maximally random jammed state of truncated tetrahedra, J. Phys. Chem. B **118**, 7981 (2014).

[13] L. Berthier, P. Chaudhuri, C. Coulais, O. Dauchot, and P. Sollich, Suppressed Compressibility at Large Scale in Jammed Packings of Size-Disperse Spheres, Phys. Rev. Lett. **106**, 120601 (2011).

[14] R. Kurita and E. R. Weeks, Incompressibility of polydisperse random-close-packed colloidal particles, Phys. Rev. E **84**, 030401 (2011).
[15] R. Dreyfus, Y. Xu, T. Still, L. A. Hough, A. G. Yodh, and S. Torquato, Diagnosing hyperuniformity in two-dimensional, disordered, jammed packings of soft spheres, Phys. Rev. E **91**, 012302 (2015).
[16] I. Lesanovsky and J. P. Garrahan, Out-of-equilibrium structures in strongly interacting Rydberg gases with dissipation, Phys. Rev. A **90**, 011603 (2014).
[17] D. Hexner and D. Levine, Hyperuniformity of Critical Absorbing States, Phys. Rev. Lett. **114**, 110602 (2015).
[18] R. L. Jack, I. R. Thompson, and P. Sollich, Hyperuniformity and Phase Separation in Biased Ensembles of Trajectories for Diffusive Systems, Phys. Rev. Lett. **114**, 060601 (2015).
[19] R. P. Feynman, Atomic theory of the two-fluid model of liquid helium, Phys. Rev. **94**, 262 (1954).
[20] R. P. Feynman and M. Cohen, Energy spectrum of the excitations in liquid helium, Phys. Rev. **102**, 1189 (1956).
[21] S. Torquato, A. Scardicchio, and C. E. Zachary, Point processes in arbitrary dimension from fermionic gases, random matrix theory, and number theory, J. Stat. Mech. Theor. Exp. (2008) P11019.
[22] C. De Rosa *et al.*, Toward hyperuniform disordered plasmonic nanostructures for reproducible surface-enhanced Raman spectroscopy, Phys. Chem. Chem. Phys. **17**, 8061 (2015).
[23] R. Degl'Innocenti *et al.*, THz quantum cascade lasers based on a hyperuniform design, Proc. SPIE **9370**, 93700A (2015).
[24] S. Yu, X. Piao, J. Hong, and N. Park, Bloch-like waves in random-walk potentials based on supersymmetry, Nat. Commun. **6**, 8269 (2015).
[25] Y. Jiao, T. Lau, H. Hatzikirou, M. Meyer-Hermann, J. C. Corbo, and S. Torquato, Avian photoreceptor patterns represent a disordered hyperuniform solution to a multi-scale packing problem, Phys. Rev. E **89**, 022721 (2014).
[26] R. D. Batten, F. H. Stillinger, and S. Torquato, Classical disordered ground states: Super-ideal gases, and stealth and equi-luminous materials, J. Appl. Phys. **104**, 033504 (2008).
[27] M. Florescu, S. Torquato, and P. J. Steinhardt, Designer disordered materials with large complete photonic band gaps, Proc. Natl. Acad. Sci. USA **106**, 20658 (2009).
[28] M. Florescu, P. J. Steinhardt, and S. Torquato, Optical cavities and waveguides in hyperuniform disordered photonic solids, Phys. Rev. B **87**, 165116 (2013).
[29] W. Man *et al.*, Isotropic band gaps and freeform waveguides observed in hyperuniform disordered photonic solids, Proc. Natl. Acad. Sci. USA **110**, 15886 (2013).
[30] O. Leseur, R. Pierrat, and R. Carminati, High-density hyperuniform materials can be transparent, Optica **3**, 763 (2016).
[31] L. S. Froufe-Pérez, M. Engel, J. José-Sáenz, and F. Scheffold, Band gap formation and Anderson localization in disordered photonic materials with structural correlations, Proc. Natl. Acad. Sci. USA **114**, 9570 (2017).
[32] G. Zhang, F. H. Stillinger, and S. Torquato, Transport, geometrical, and topological properties of stealthy disordered hyperuniform two-phase systems, J. Chem. Phys. **145**, 244109 (2016).
[33] D. Chen and S. Torquato, Designing disordered hyperuniform two-phase materials with novel physical properties, Acta Mater. **142**, 152 (2018).
[34] G. Zhang, F. H. Stillinger, and S. Torquato, Can exotic disordered "stealthy" particle configurations tolerate arbitrarily large holes? Soft Matter **13**, 6197 (2017).
[35] S. Torquato, Hyperuniform states of matter, arXiv:1801.06924 [Phys. Rep. (to be published)].
[36] S. Torquato, *Random Heterogeneous Materials: Microstructure and Macroscopic Properties* (Springer-Verlag, Berlin, 2002).
[37] S. Torquato and F. H. Stillinger, Jammed hard-particle packings: From Kepler to Bernal and beyond, Rev. Mod. Phys. **82**, 2633 (2010).
[38] Y. Jiao, F. H. Stillinger, and S. Torquato, A superior descriptor of random textures and its predictive capacity, Proc. Natl. Acad. Sci. USA **106**, 17634 (2009).
[39] R. A. DiStasio, Jr., É. Marcotte, R. Car, F. H. Stillinger, and S. Torquato, Designer spin systems via inverse statistical mechanics, Phys. Rev. B **88**, 134104 (2013).
[40] É. Marcotte, R. A. DiStasio, Jr., F. H. Stillinger, and S. Torquato, Designer spin systems via inverse statistical mechanics. II. Ground-state enumeration and classification, Phys. Rev. B **88**, 184432 (2013).
[41] E. Chertkov, R. A. DiStasio, Jr., G. Zhang, R. Car, and S. Torquato, Inverse design of disordered stealthy hyperuniform spin chains, Phys. Rev. B **93**, 064201 (2016).
[42] E. Ising, Beitrag zur theorie des ferromagnetismus, Z. Phys. **31**, 253 (1925).
[43] S. G. Brush, History of the Lenz-Ising model, Rev. Mod. Phys. **39**, 883 (1967).
[44] P. J. Steinhardt, D. R. Nelson, and M. Ronchetti, Bond-orientational order in liquids and glasses, Phys. Rev. B **28**, 784 (1983).
[45] M. D. Rintoul and S. Torquato, Metastability and Crystallization in Hard-Sphere Systems, Phys. Rev. Lett. **77**, 4198 (1996).
[46] A. R. Kansal, T. M. Truskett, and S. Torquato, Non-equilibrium hard-disk packings with controlled orientational order, J. Chem. Phys. **113**, 4844 (2000).
[47] T. M. Truskett, S. Torquato, and P. G. Debenedetti, Towards a quantification of disorder in materials: Distinguishing equilibrium and glassy sphere packings, Phys. Rev. E **62**, 993 (2000).
[48] Y. Jiao, F. H. Stillinger, and S. Torquato, Modeling heterogeneous materials via two-point correlation functions: Basic principles, Phys. Rev. E **76**, 031110 (2007).
[49] E. Lomba, J. J. Weis, and S. Torquato, Disordered hyperuniformity in two-component non-additive hard disk plasmas, Phys. Rev. E **96**, 062126 (2017).
[50] S. Franz and G. Parisi, Local spin glass order in 1D, Europhys. Lett. **75**, 385 (2006).
[51] S. Franz, H. Jacquin, G. Parisi, P. Urbani, and F. Zamponi, Quantitative field theory of the glass transition, Proc. Natl. Acad. Sci. USA **109**, 18725 (2012).
[52] T. Caelli, On discriminating visual textures and images, Percept. Psychophys. **31**, 149 (1982).
[53] S. Torquato, G. Zhang, and M. De Courcy-Irleland, Uncovering multiscale order in the prime numbers via scattering, Sci. Adv. (unpublished).
[54] S. Kirkpatrick, C. D. Gelatt, and M. P. Vecchi, Optimization by simulated annealing, Science **220**, 671 (1983).

[55] M. Vaezi, H. Seitz, and S. Yang, A review on 3D micro-additive manufacturing technologies, Int. J. Adv. Manuf. Technol. **67**, 1721 (2013).

[56] E. D. Protonotarios, A. Johnston, and L. D. Griffin, Difference magnitude is not measured by discrimination steps for order of point patterns, J. Vis. **16**, 2 (2016).

[57] K. He, X. Zhang, S. Ren, and J. Sun, Delving deep into rectifiers: Surpassing human-level performance on imagenet classification, in *Proceedings of the IEEE International Conference on Computer Vision* (IEEE, New York, 2015), pp. 1026–1034.

[58] C. E. Shannon, A mathematical theory of communication, Bell Syst. Tech. J. **27**, 379 (1948).

[59] A. Kolmogorov, On tables of random numbers, Theor. Comput. Sci. **207**, 387 (1998).

[60] P. Grunwald and P. Vitanyi, Shannon information and Kolmogorov complexity, arXiv:cs/0410002.

[61] V. Katos, A randomness test for block ciphers, Appl. Math. Comput. **162**, 29 (2005).

[62] Y. Meyer, *Wavelets and Operators* (Cambridge University Press, Cambridge, UK, 1992).